CHEMISTRY
A EUROPEAN JOURNAL

DOI: 10.1002/chem.200701527

Single-Crystal X-ray Study of $Ba_2Cu_2Te_4O_{11}Br_2$ and Its Incommensurately Modulated Superstructure Companion

Rie Fredrickson Takagi, Mats Johnsson, and Sven Lidin*[a]

Abstract: Compounds containing lone-pair elements such as Te^{IV} are very interesting from the structural point of view, as the lone-pair nonbonding regions create low-dimensional geometrical arrangements. We have synthesized two new compounds with these features—$Ba_2Cu_2Te_4O_{11}Br_2$ (**I**) and $Ba_2Cu_2Te_4O_{11-\delta}(OH)_{2\delta}Br_2$ (**II**, $\delta \approx 0.57$)—as members of the AE-M-Te-O-X (AE = alkaline-earth metal, M = transition metal, X = halide) family of compounds by solid-state reactions. Preliminary single-crystal X-ray analysis indicated that compound **I** crystallizes in the orthorhombic system, but attempts at refinement proved unsatisfactory. Closer inspection of the reciprocal lattice revealed systematic, non-crystallographic absences that indicate twinning. The structure is in fact triclinic, space group $C\bar{1}$ (equivalent to $P\bar{1}$), with unit cell parameters (at 120 K) of $a = 10.9027(9)$, $b = 15.0864(7)$, $c = 9.379(2)$ Å, $\beta = 106.8947°$. It is layered and built from $[TeO_3E]$ tetrahedra, $[TeO_{3+1}E]$ trigonal bipyramids (where E is the lone pair of Te^{IV}), $[CuO_4]$ squares and irregular $[BaO_{10}Br]$ polyhedra. The crystal structure of **II** shows the same basic structure as **I** but contains additional oxygen, probably in the form of OH groups. The presence of satellites reveals that ordering on this O site creates an incommensurate modulation, primarily affecting Br and Te. The modulated structure of **II** was solved in the triclinic superspace group $X\bar{1}(\alpha\beta\gamma)0$ with the vector $\boldsymbol{q} \approx 1/16\,\boldsymbol{c}^*$.

Keywords: alkaline earth metals · layered compounds · solid-state reactions · structure elucidation · tellurium

Introduction

Metal oxide halides containing elements with stereochemically active lone pairs, for example, Te^{IV}, Se^{IV}, As^{III}, and Sb^{III}, have proven to be an attractive research field for finding a family of novel compounds with rich structural chemistry. For such compounds in the L-M-O-X system (L: elements bearing a stereo-active lone pair, M: transition metal, X: halogen) there is a high probability of finding low-dimensional arrangements of the transition metals such as layers (2D) or chains (1D),[1] which may lead to interesting physical properties, for example, high-temperature superconductivity (HTSC) and antiferromagnetic spin frustration.[2] In this system, the combination of the lone pair on the Te^{IV} atom and the halogens constitute "structural scissors" that hinder the development of three-dimensional networks. In most oxide chlorides and oxide bromides, the lone-pair elements are more "oxophilic" and tend to be coordinated by the oxygen atoms, while the late transition metals are coordinated by both oxygen and halogen atoms. Introducing an alkaline earth element (AE) is another structural strategy for forming low-dimensional arrangements of the transition metal substructure. The AEs are known for their flexible coordination and can bond to equally well to oxygen and halogens, and when the AE forms two-dimensional layers it separates one transition metal unit from the next and thus blocks the propagation of, for example, magnetic coupling.

The present work is an outcome of an ongoing investigation of transition metal oxide halides containing asymmetrically coordinated lone-pair elements and an alkaline earth element. The crystal structures of a few compounds in this family of AE-Te-M-O-X compounds have been described before: $Ba_2Co(SeO_3)_2Cl_2$,[2] $Ba_2Cu_4Te_4O_{11}Cl_4$ and $BaCu_2Te_2O_6Cl_2$.[3] Additionally, a compound that does not strictly belong to this family (no transition metal element is present), $Ba_3Te_2O_6Cl_2$, which contains similar Ba-centered slabs, has been reported.[4] This is the first case in which an incommensurately modulated structure has been observed for a member of the AE-M-Te-O-X family. The new com-

[a] R. Fredrickson Takagi, M. Johnsson, S. Lidin
Inorganic Chemistry
Stockholm University
10691 Stockholm (Sweden)
Fax: (+46) 8-15-21-87
E-mail: takagi@inorg.su.se
matsj@inorg.su.se
sven@inorg.su.se

pounds $Ba_2Cu_2Te_4O_{11}Br_2$ (**I**) and $Ba_2Cu_2Te_4O_{11-\delta}(OH)_{2\delta}Br_2$ (**II**, $\delta \approx 0.57$) formed in solid-phase/gas-phase reactions as layered crystal structures in which only weak van der Waals forces exist between layers.

Experimental Section

BaO (Sigma Aldrich, +99.9%), $CuBr_2$ (Avocado Research Chemicals, +98%), CuO (Avocado Research Chemicals, +99%) and TeO_2 (ABCR, +99%) were used as starting materials for the synthesis of $Ba_2Cu_2Te_4O_{11}Br_2$ (**I**) and $Ba_2Cu_2Te_4O_{11-\delta}(OH)_{2\delta}Br_2$ (**II**, $\delta \approx 0.57$). For **I**, a mixture of BaO, $CuBr_2$, CuO and TeO_2 in 2:1:1:4 stoichiometric molar ratio were pressed together into a tablet which was then sealed in an evacuated silica tube (length ca. 5 cm) and heated at 600 °C for 120 h. This procedure resulted in a mixture of black and light green powder and green, transparent, prismatic crystals of **I**. For **II**, the starting materials, in 1:1:1:2 non-stoichiometric molar ratio were prepared in a glove box, sealed in in a silica tube under vacuum and heated at 650 °C for 65 h in a muffle furnace. The product was a mixture of black and yellow powders and green, transparent, prismatic crystals of **II**. The crystals from both syntheses were approximately $0.3 \times 0.4 \times 0.5$ nm in size and non-hygroscopic.

Table 1. Crystal data, data collection, and refinement parameters for $Ba_2Cu_2Te_4O_{11}Br_2$ (**I**) and $Ba_2Cu_2Te_4O_{11-\delta}(OH)_{2\delta}Br_2$ ($\delta \approx 0.57$) (**II**).

empirical formula	$Ba_2Cu_2Te_4O_{11-\delta}(OH)_{2\delta}Br_2$ ($\delta \approx 0.57$)	$Ba_2Cu_2Te_4O_{11}Br_2$
molar mass [g mol^{-1}]	1250.4	1248
temperature of measurement [K]	293	120
wavelength	0.71069	0.71069
space group (no.)	$X\bar{1}(\alpha\beta\gamma)0$	$C\bar{1}$ (no. 2)
unit cell dimensions		
a [Å]	10.9121(5)	10.9027(9)
b [Å]	15.1015(6)	15.0864(7)
c [Å]	9.413(2)	9.379(2)
α [°]	90	90
β [°]	106.8468	106.8947
γ [°]	90	90
V [Å^3]	1484.6(3)	1476.1(3)
$\boldsymbol{q}$ vector	$\approx 1/16\,\boldsymbol{c}^*_{tric}$	–
Z	4	4
$F(000)$	2149	2144
ρ_{calcd} [g cm^{-3}]	5.5927	5.6138
absorption coefficient	21.194	21.315
range of θ [°]	3.76–33.35	3.91–36.42
observed reflections [$I > 3\sigma(I)$]	6813	6591
independent reflections	4923	4392
R_{int} (obs/all) [%]	4.78/5.22	2.89/3.10
number of parameters	103	136
R_1 (obs/all) [%]	4.82/7.13	3.14/5.14
R_{main}(obs) [%]	3.01	–
$R_{1st\,sat}$(obs) [%]	7.89	–
wR(obs/all) [%]	4.66/4.92	4.21/4.50
absorption correction	multiscan	multiscan
index ranges	$-16 \le h \le 16$	$-17 \le h \le 18$
	$-22 \le k \le 22$	$-25 \le k \le 24$
	$-14 \le l \le 14$	$-15 \le l \le 15$
completeness [%] to θ [°]	95, $\theta = 22.29$	95, $\theta = 35.42$
refinement method	full-matrix least-squares on F	full-matrix least-squares on F
GoF on F^2	1.73	1.19
largest diff. peak and hole [e Å^{-3}]	−4.67, 4.62	−2.41, 3.43

Single-crystal X-ray diffraction data were collected for **I** at 120, 297 and 373 K and for **II** at ambient temperature on an Oxford Diffraction Xcalibur3 diffractometer using graphite-monochromatized $Mo_{K\alpha}$ radiation ($\lambda = 0.71069$ Å). The intensities of the reflections were integrated by using the CrysAlis Red software[5] supplied by the manufacturer. Numerical absorption correction was performed with the programs CrysAlis RED.[5] The structures were solved by direct methods using the program SHELXS97[6] and refined by full-matrix least-squares techniques on F using the program JANA2000.[7] All fully occupied position except for oxygen (**I**) and copper and oxygen (**II**) were refined with anisotropic temperature parameters. Molecular graphics were prepared with the program DIAMOND.[8] Crystal data for **I** and **II** are reported in Table 1. Further details of the crystal structure investigations may be obtained from the Fachinformationszentrum Karlsruhe, 76344 Eggenstein-Leopoldshafen, Germany (fax: (+49) 7247-808-666; e-mail: crysdata@fiz-karlsruhe.de) on quoting the depository numbers CSD-418628 ($Ba_2Cu_2Te_4O_{11}Br_2$, data collected at 120 K) and CSD-418630 $Ba_2Cu_2Te_4O_{11-\delta}(OH)_{2\delta}Br_2$ ($\delta \approx 0.57$).

The chemical composition (metal content only) of the products was confirmed by energy-dispersive spectroscopy (EDS, LINK AN10000) in a scanning electron microscope (SEM, JEOL820) operated at 20 kV.

Results and Discussion

Newly synthesized compound $Ba_2Cu_2Te_4O_{11}Br_2$ (**I**) and its incommensurately modulated companion $Ba_2Cu_2Te_4O_{11-\delta}(OH)_{2\delta}Br_2$ (**II**, $\delta \approx 0.57$) belong to the family AE-Te-M-O-X. The structures of such compounds are receiving attention due to the interesting tendency of stereochemically active lone pairs to form low-dimensional arrangements. This is often observed as regions of strong bonding connectivity segregated by non-bonding regions to create layer (2D), column (1D) or cluster (0D) arrangements. Compounds **I** and **II** are two-dimensional, layered and have is no strong connection between the layers. Characterization of the structural features of this family, and the physical properties that arise from them, is the subject of on-going research.

Structural analysis on basic cell: A preliminary single-crystal X-ray diffraction experiment on **I** revealed a pronounced B-centered orthorhombic subcell ($a = 5.4511$, $b = 7.5412$, $c = 17.9522$ Å) with superstructure reflections doubling the $<111>$ directions to yield an F-centered orthorhombic cell ($a = 10.9121(5)$, $b = 15.1011(6)$, $c = 36.0363(15)$ Å).

Attempts at a structural solution in the subcell (space group $Bmmb$) quickly yield an average structure with composition $BaTe_2CuBrO_5$, and an additional oxygen position with partial ($^1/_2$) occupancy. The superstructure cell shows

systematic absences in addition to those associated with *F*-centering. In particular, the extinction conditions $0kl$: $k+l=4n$ and $h0l$: $h+l=4n$ strongly suggest the space group *Fdd*2. Ordering the occupancy of the extra oxygen atom in the 2*2*2 super cell and *Fdd*2 symmetry does yield a reasonable solution, but many atom positions remain split and refinement does not converge satisfactorily.

Closer examination of the diffraction pattern reveals non-crystallographic extinction conditions. The *B*-centering from the subcell is perfectly preserved, as is *F*-centering in the supercell. This means that the subcell reflections obey the additional condition $h2nl$: $h+l=4n$. This is a strong indication of twinning. The *B*-centered, orthorhombic subcell can be transformed into a primitive monoclinic cell with $a=5.4511$, $b=7.5412$, $c=9.3808$ Å, $\beta=106.891°$ (Figure 1) by matrix $\mathbf{M}_1$ [Eq. (1)].

$$\mathbf{M}_1 = \begin{pmatrix} 1 & 0 & 0 \\ 0 & 1 & 0 \\ -\frac{1}{2} & 0 & \frac{1}{2} \end{pmatrix}$$

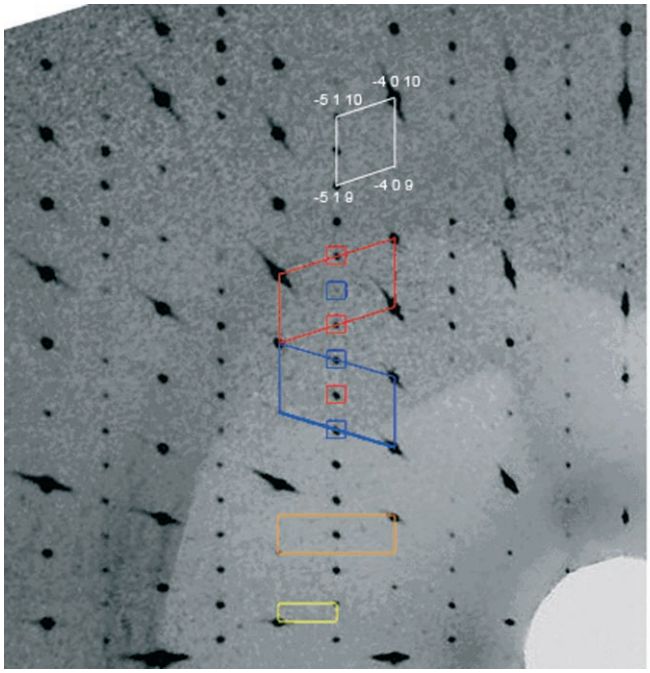

Figure 1. X-ray diffraction image of compound **I** indexed as the *C*-centred triclinic cell (white; $a=10.9027(9)$, $b=15.0864(7)$, $c=9.379(2)$ Å, $\beta=106.8947°$). Additionally, the *C*-centered twinned monoclinic cell (red or blue; $a=5.4511$, $b=7.5412$, $c=9.3808$ Å, $\beta=106.891°$), the orthorhombic *B*-centered subcell (orange; $a=5.4511$, $b=7.5412$, $c=17.9522$ Å) and *F*-centered 2*2*2 super cell (yellow; $a=10.9121(5)$, $b=15.1011(6)$, $c=36.0363(15)$ Å) are shown. The image shows a reconstructed slab of reciprocal space encompassing the $h0l$ and $h1l$ planes. A projection of the full reciprocal lattice would look very similar

The fact that the superstructure reflections occur with a frequency twice that of the basic-structure reflections along the orthorhombic c^* direction can now be interpreted as superstructure-induced twinning; these twinned monoclinic unit cells are showed in red and blue in Figure 1. These two cells share the same reciprocal lattice but have distinct superstructure reflections along their respective c^* directions, highlighted in the figure by red and blue boxes. It seems highly probable that the crystal is indeed a balanced twin of two equivalent modes of superstructure. Note that the image in Figure 1 is in fact not a section of reciprocal space, but slabs extending from the $h0l$ layer to the $h1l$ layer, that is, the sum of the two reciprocal lattice layers $h0l$ and $h1l$. While only reflections from the basic structure are present in $h0l$, only superstructure reflections are present in $h1l$, and so the doubling in the *ac* plane is always accompanied by simultaneous doubling of the *b* axis. The unit cell used for further work was generated by doubling *a* and *b* directions of the monoclinic cell above, and this leads to a *C*-centered cell. Systematic absences indicate the maximal symmetry to be $C2/m$. Twin refinement in this space group yields a reasonable, but not quite satisfactory result, and so further symmetry reduction was tried. Neither the space group *C*2 nor *C*m resolved the issues, but finally, a solution without any disturbing residuals, and with excellent agreement between diffraction data and model was achieved for a triclinic, centrosymmetric solution, here given in the nonstandard setting space group $C\bar{1}$ ($a=10.9027(9)$, $b=15.0864(7)$, $c=9.379(2)$ Å, $\beta=106.8947°$).

All positions, save that corresponding to the extra oxygen atom (O11), represent nothing but a more or less pronounced deviation from the solution in the *Bmmb* subcell, but the distribution of O11 on this highly symmetric matrix disrupts all symmetry apart from the center of inversion. This massive symmetry breaking from the single oxygen position may appear surprising, but it is in fact quite straightforward. A full symmetry analysis would require a rather tedious exhaustive procedure, but if we assume that a center of symmetry should indeed be present, the analysis can be limited to two simple cases. In Figure 2, only the Ba atoms and O11 are shown in the setting of a monoclinic cell. The O11 atoms form pairs with an atom-to-atom separation of 4.3 Å. The axes of the pair are collinear and inclined with respect to the *b* axis, effectively precluding any reflection symmetry perpendicular to that axis. Since the monoclinic *b* axis is also an axis of the orthorhombic cell, the same argument applies to the orthorhombic case. Since we assume that a center of symmetry is present, this also forbids the presence of any twofold rotational symmetry (2 or 2_1) along *b*, and so the symmetry cannot be either orthorhombic or monoclinic with a unique *b* axis.

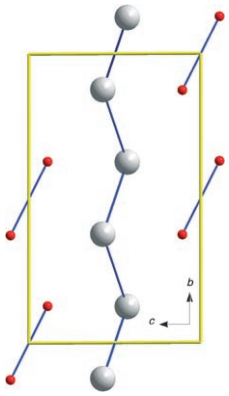

Figure 2. Projection of the substructure of Ba and O11 along the (pseudo)monoclinic *a* axis. Note the inclination of O11 pairs that effectively rules out any reflections perpendicular to *b*.

The twinning apparent in the diffraction pattern leading to pseudo-orthorhombic symmetry refined to a value close to 50 %

for each of the two components. Introduction of new subvolumes with orientations corresponding to the symmetry reduction from monoclinic to triclinic was attempted, but these subvolumes quickly converged to zero in the refinement. An indication that the triclinic/monoclinic symmetry breaking does not lead to any balanced twinning is the fact that the triclinic R_{int} is substantially better (3%) than the monoclinic R_{int} value of 10%. In the final model, only two subvolumes where used, and their relative sizes were set equal.

Atomic coordinates and selected interatomic distances are listed in Tables 2 and 3. All metal atoms have classical coordination environments. The Te atoms exhibit two kinds of coordination environments: three-fold, one-sided $[TeO_3]$ pyramids and $[TeO_{3+1}]$ see-saw coordination (Figure 3a and b). If the lone pair is taken into account these coordination figures become tetrahedra and trigonal bipyramids, respectively. Lone pairs were placed according to the procedure used by Galy et al.[9] The Ba atoms are surrounded by ten oxygen atoms in an irregular 4+6 arrangement (Figure 3c). For Cu the arrangement is square-planar (oxygen) with an additional apical Br atom at a longer distance (Figure 3d).

While the oxygen coordination is straightforward, it is useful to refer to bond valence sum (BVS) calculations[10] to understand the role of Br. The BVS suggests that the Br ions do not contribute significantly to the bonding for either Cu or Ba, and should be considered more as charge-compensating ions than halide ligands.

The $[TeO_3E]$ and $[TeO_{3+1}E]$ units build up $[Te_4O_{11}E_4]$ chains by sharing corners along the $\langle 010 \rangle$ direction. The $[Te_4O_{11}E_4]$ chains are linked by $[CuO_4]$ units to form Cu-Te-O layers that are connected via $[BaO_{10}]$ polyhedra to form slabs. These $[Ba_2Cu_2Te_4O_{11}]^{2-}$ slabs are identical to those found in $Ba_2Cu_2Te_4O_{11}Cl_4$,[3] which was prepared from NH_4Cl solution. The difference between the two compounds lies only in the species located between the layers, and the relative position and orientation of the layers with respect to each other. This similarity is an interesting parallel to that between cubic Sb_2O_3 and the recently prepared compound Sb_2O_3CuBr, in which a puckered CuBr network interleaves slabs of c-Sb_2O_3, which shows the flexibility of separated lone-pair layers in accommodating halidic structural elements.[11] An overview of the structure of **I** is shown in Figure 4. The Br atoms form infinite columns between the Te lone pairs.

It would be interesting to characterize the magnetic properties of this low-dimensional compound with diluted $[CuO_4]$ square planes that are not in contact and thus imply the existence of only weak super–super exchange coupling between the Cu atoms. However, so far we have not succeeded in preparing a monophasic powder of $Ba_2Cu_2Te_4O_{11}Br_2$ for magnetic susceptibility measurements.

Table 3. Interatomic distances [Å] for $Ba_2Cu_2Te_4O_{11}Br_2$ (**I**) measured at 120 K.

Atoms		Distance	Atoms		Distance
Te1	O3	1.847(7)	Cu2	Br1	3.031(1)
Te1	O6	1.900(11)			
Te1	O9	1.885(5)	Ba1	O1	2.791(10)
Te2	O5	1.854(7)	Ba1	O3	2.908(9)
Te2	O7	1.901(9)	Ba1	O3	2.943(8)
Te2	O10	1.910(4)	Ba1	O4	2.875(8)
Te3	O1	1.919(11)	Ba1	O5	2.942(9)
Te3	O8	1.859(7)	Ba1	O6	2.945(9)
Te3	O10	2.292(4)	Ba1	O7	2.825(7)
Te3	O11	1.975(5)	Ba1	O7	2.863(9)
Te4	O2	1.906(9)	Ba1	O9	2.870(8)
Te4	O4	1.845(7)	Ba1	O10	2.938(8)
Te4	O9	2.310(5)	Ba1	Br2	3.512(1)
Te4	O11	1.959(5)	Ba2	O1	2.945(8)
			Ba2	O2	2.854(9)
Cu1	O1	1.987(9)	Ba2	O2	2.869(8)
Cu1	O2	1.997(9)	Ba2	O4	2.989(8)
Cu1	O3	1.937(9)	Ba2	O5	2.896(9)
Cu1	O5	1.925(9)	Ba2	O6	2.816(10)
Cu1	Br2	3.027(1)	Ba2	O8	2.887(10)
Cu2	O4	1.942(8)	Ba2	O8	2.905(8)
Cu2	O6	1.982(10)	Ba2	O9	2.993(9)
Cu2	O7	1.978(8)	Ba2	O10	2.824(8)
Cu2	O8	1.937(9)	Ba2	Br1	3.506(1)

Table 2. Fractional atomic coordinates, occupancies and isotropic ADPs for $Ba_2Cu_2Te_4O_{11}Br_2$ (**I**) measured at 120 K. The Ba, Te, and Br atoms were refined by using anisotropic ADPs (italics). All atoms are fully occupied and their Wyckoff positions are 4b.

Element	Atom	x	y	z	U_{iso}/U_{eq} [Å^2]
Ba	Ba1	0.8588(1)	0.12402(3)	0.42856(4)	*0.0053(2)*
Ba	Ba2	0.8571(1)	−0.37501(3)	0.42951(4)	*0.0053(2)*
Te	Te1	0.5551(1)	0.23783(3)	0.21177(5)	*0.0058(1)*
Te	Te2	0.5546(1)	−0.48870(3)	0.21422(5)	*0.0050(1)*
Te	Te3	0.4485(1)	−0.75315(3)	−0.19828(5)	*0.0050(1)*
Te	Te4	0.4518(1)	0.00806(3)	−0.19418(5)	*0.0054(1)*
Br	Br1	0.7688(1)	−0.12402(6)	−0.0404(1)	*0.0155(3)*
Br	Br2	0.79030(8)	0.12376(6)	0.0388(1)	*0.0120(3)*
Cu	Cu1	0.3239(2)	−0.12562(5)	0.29640(9)	*0.0055(3)*
Cu	Cu2	0.1770(2)	0.12548(5)	−0.29544(9)	*0.0056(3)*
O	O1	0.4536(8)	−0.2220(6)	0.334(1)	0.008(2)
O	O2	0.4590(7)	−0.0319(6)	0.3372(9)	0.007(2)
O	O3	0.2933(7)	−0.2857(6)	−0.3295(9)	0.003(2)
O	O4	0.2911(7)	0.0320(6)	−0.3211(8)	0.003(2)
O	O5	0.2104(7)	−0.0346(6)	0.3269(9)	0.005(2)
O	O6	0.0462(8)	0.2207(7)	−0.322(1)	0.010(2)
O	O7	0.5402(7)	0.5347(6)	−0.3387(9)	0.006(2)
O	O8	0.7919(7)	−0.2848(6)	0.669(1)	0.004(2)
O	O9	0.5845(8)	0.1280(3)	0.3118(5)	0.0072(9)
O	O10	0.5869(7)	−0.3797(3)	0.3221(5)	0.0036(8)
O	O11	0.5269(7)	−0.1274(3)	0.1081(5)	0.0068(8)

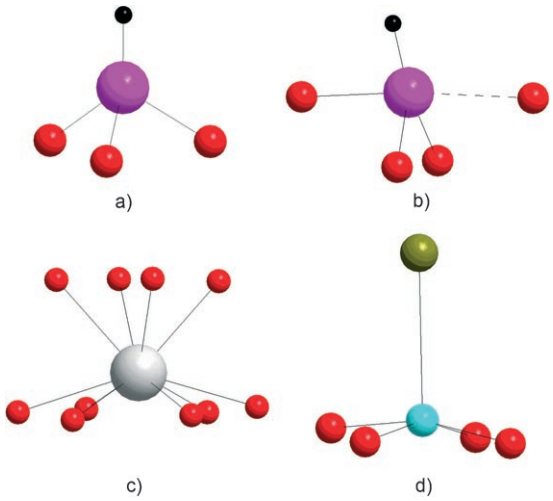

Figure 3. Local coordination polyhedra for Te (a and b), Ba (c) and Cu (d)

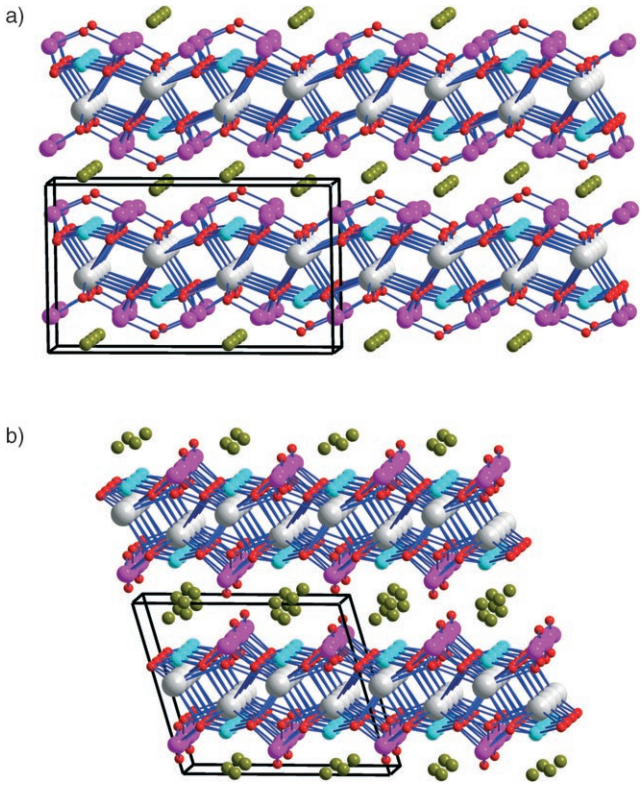

Figure 4. Structure of **I** in the triclinic space group $C\bar{1}$, pseudomonoclinic setting. Color code: Ba silver, Te pink, Cu cyan, O red, Br olive green. The c^* direction is vertical in both pictures. a) View along a direction close to *a*. Note how the structure is composed of slabs centered by Ba, and how the non-bonding side of Te interfaces with the Br region. The Br positions form almost perfectly straight lines along *a*. b) View along a direction close to *b*. Note the relaxation of the Br positions along *c*.

Modulated superstructure: In the single-crystal X-ray diffraction pattern of **II**, the superstructure reflections seen in **I** are split along c^*_{tric} (Figure 5). The structure was assumed to be similar to that of **I**, and consequently the diffraction pattern was indexed by using the same basic cell. The fact that the superstructure reflections (hkl, $k=2n+1$) of **I** are absent and replaced by a pair of satellites is best described by a centering condition X, $hklm$, $h+k+m=2n$, indicative of a centering vector ($^1/_2{}^1/_2 0 {}^1/_2$). Using the structure of compound **I** in triclinic setting as a non-modulated starting model resulted in large displacement parameters on the Br atoms, and as a consequence, these were used to phase the satellite reflections.

The position O6 in **II**, which corresponds to O11 in **I**, was expected to show partial occupancy. Indeed, if the structure of **I** is described in this 3+1 dimensional setting, the position O6 must be half-occupied. Interestingly, the occupation of O6 refines to a value significantly larger than $^1/_2$, about 0.57. The Te atoms also show significant positional modulations. This seems to indicate that the oxygen position has higher occupancy in **II** than in **I**. This is a little surprising, considering the oxidation states of the elements in the structure. It is difficult to imagine the oxidation of divalent Ba or Cu, and the oxidation of Te^{4+} to Te^{6+} always leads to a dramatically different coordination. The most plausible explanation is therefore that some O^{2-} on position O6 has been replaced by OH^-, which allows for higher occupancy without any redox activity.

Examining the local details of the modulated structure supports this explanation. The bond valence sum of O6 has a maximum around 2.2 and then drops towards unity before the square wave type occupation function switches to zero (Figure 6), and the position of the Br ion changes conspicuously with the modulation. When O6 is present on one side of the Br atom, the Br atom is displaced from the symmetric locus, and the Br–O distance has its maximum of around

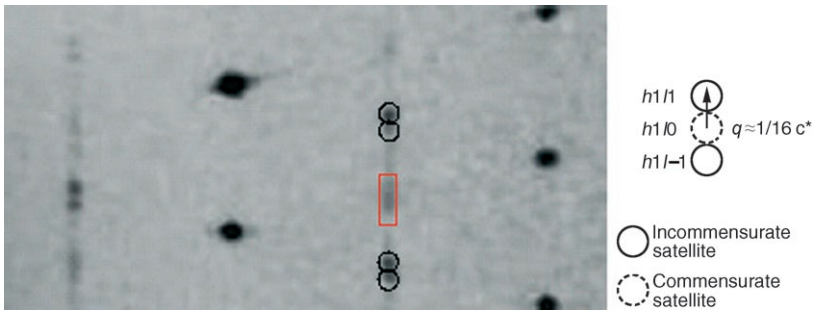

Figure 5. Superstructure reflections of incommensurate **II** are shown with the split reflections ($h0lm$, $m=1$, -1). The position of the superstructure reflection in the commensurate compound is indicated by a dashed circle. The reciprocal reconstructions are sums of $h0l$ and $h1l$ plane. Note the presence of twinning also in the modulated structure. The satellites in the red rectangle emanate from a second, smaller and less well crystallized individual. This is analogous to the second individual seen in Figure 1.

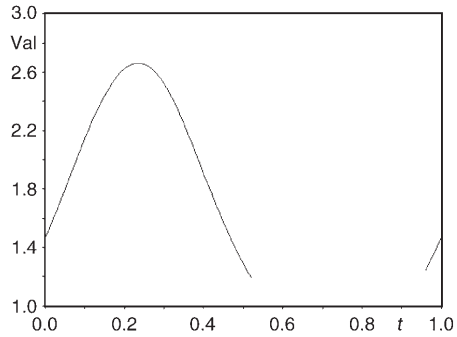

Figure 6. Bond valence sum for O6. Note how the BVS approaches the ideal value of two close to the center of the existence domain which represents a lone O6, while at the edges of that domain the BVS drops towards 1. The O6 atoms corresponding to this position form pairs that straddle a Br ion with short distances. Distances and BVS together suggest the presence of OH^- groups.

3.5 Å. When O6 is present on both sides, the Br atom is forced into a symmetric position with two rather short (3.0 Å) Br–O distances (Figure 7). In $HBr{\cdot}2H_2O$ hydrogen-

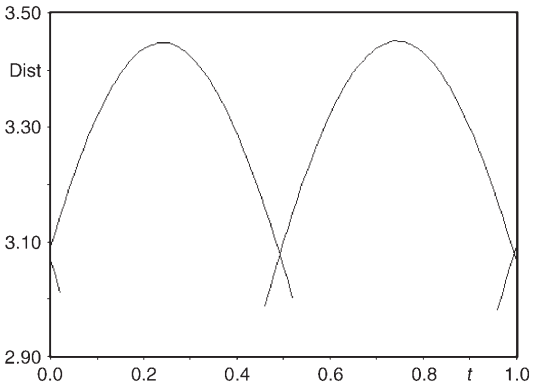

Figure 7. Distance plot for Br–O6. Note the anomalous presence of two O6 atoms at distances close to Br, or a single O6 atom at a larger distance.

bridged Br–O distances are 3.2 Å, while unbridged contacts tend to be 0.5 Å longer,[12] and in $NaBr{\cdot}2H_2O$ the pattern is the same.[13] While the Br–O distances in **II** are on the short side, there is an indication that the shortest contacts could be H-mediated.

The model imported from $Ba_2Cu_2Te_4O_{11}Br_2$ includes the pseudo-merohedral orthorhombic/monoclinic twinning. For the modulated compound this, however, proved to be insufficient, and it was necessary to take monoclinic/triclinic twinning into account as well. This led to a major reduction in R values for satellites (from 25 to 8%). In the final refinement in the triclinic superspace group $X\bar{1}(\alpha\beta\gamma)0$ with the vector $\boldsymbol{q}\approx 1/16\,\boldsymbol{c}^*_{tric}$ (approximation of the incommensurately modulated superstructure is shown in Figure 8), 103 parameters were used to model about 5000 observed reflections with residual values $R_{(obs/all)}$ of 3.0/4.2 for main reflections and 7.89/11.33 for satellites. In the final refinement, in

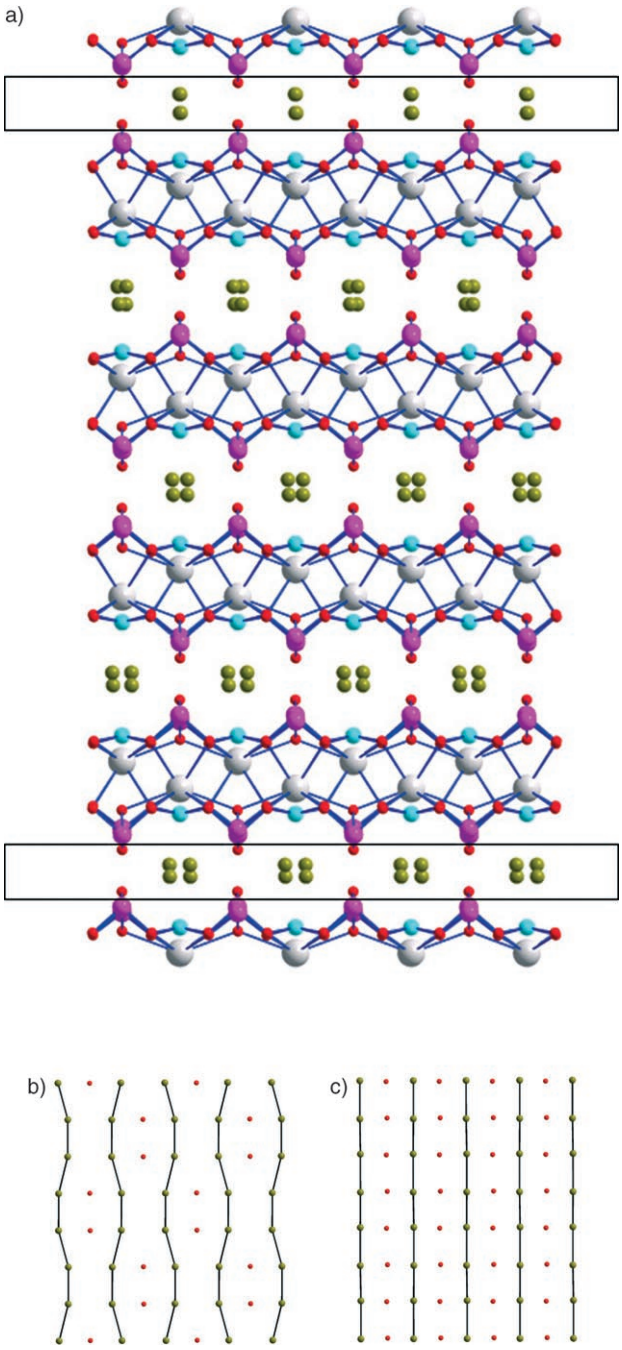

Figure 8. a) An interpretation of the incommensurately modulated superstructure model, projected along *b*. The horizontal direction is *a*. Color codes as for Figure 4b. Note how the structure, save for the Br positions, is indistinguishable from the basic structure in Figure 4b. At the bottom of the image is a region with single O6 positions, and here the projected lateral separation between Br atoms is large. This indicates a large amplitude of the displacive modulation of Br along the *a* direction. Towards the top of the image, shrinkage of the lateral separation indicates the presence of O6 on both sides of each Br, which minimizes the displacements. c) Sections in the *bc* plane of the modulated structure. The sections correspond to the rectangles at the bottom (b) and top (c) of image a). Note how the presence of extra oxygen in the layer shown in c) forces Br to remain in the highly symmetric position and attain short Br–O distances, while the sparser arrangement in b) allows for relaxation.

addition to a square-wave occupancy modulation for O6, second-order harmonic waves for positional modulation of Te and Br were used. Two sets of correlations made refinement difficult. First, the two Te positions are related by a pseudo-translation, and their anisotropic displacement parameters correlated very strongly. Therefore, these were coupled. Additionally, the twin ratios correlate with the anisotropic thermal parameters of all heavy atoms. Therefore, twin ratios and anisotropic parameters were refined alternatingly until each converged. In the final cycle, twin ratios were kept constant, and thermal parameters were refined. The fractional atomic coordinates are given in Table 4, the amplitudes of harmonic positional modulation waves in Table 5 and the occupation modulation functions of the O6 site in Table 6. The functions of the most important contributors to the modulation, Br and O6, are shown in Figure 9.

Table 4. Fractional atomic coordinates and isotropic ADPs for $Ba_2Cu_2Te_4O_{11-\delta}(OH)_{2\delta}Br_2$ ($\delta \approx 0.57$) (**II**).

Element	Atom	Occ.	x	y	z	U_{iso}/U_{eq} [Å^2]
Ba	Ba1	1	0.60726(5)	0.12442(9)	0.42878(4)	0.0092(1)
Te	Te1	1	0.30088(6)	0.24541(5)	0.20315(9)	0.0051(1)
Te	Te2	1	0.30181(6)	−0.49911(5)	0.2070(1)	0.0051(1)
Br	Br1	1	0.4892(2)	−0.1227(2)	−0.03961(9)	0.0168(3)
Cu	Cu1	1	0.0739(1)	−0.1251(2)	0.29575(8)	0.0096(2)
O	O1	1	0.2088(8)	−0.2164(5)	0.3360(9)	0.007(2)
O	O2	1	0.2029(9)	−0.0328(6)	0.323(1)	0.014(2)
O	O3	1	0.0404(8)	−0.2831(5)	−0.3374(9)	0.006(2)
O	O4	1	0.0410(9)	0.0326(6)	−0.3236(9)	0.013(2)
O	O5	1	0.3294(6)	0.125(1)	0.3157(4)	0.0128(8)
O	O6[a]	0.57(1)	0.2770(8)	−0.1261(8)	0.1092(7)	0.015(2)

[a] *O6 in **II** corresponds to O11 in **I**.

Table 5. Amplitudes of harmonic positional modulation waves refined for **II**.[a]

Atom	S_{sinx1}	S_{siny1}	S_{sinz1}	C_{cosx1}	C_{cosy1}	C_{cosz1}
Te1	0.00301(9)	−0.01252(6)	0.0109(1)	0.00013(8)	−0.00026(9)	0.0003(1)
Te2	0.00503(8)	0.01523(6)	0.01534(9)	0.00009(8)	0.00027(9)	0.0003(1)
Br	0.0443(1)	0.0005(1)	0.0000(2)	0.0024(3)	0.0000(1)	−0.0002(2)
Atom	S_{sinx2}	S_{siny2}	S_{sinz2}	C_{cosx2}	C_{cosy2}	C_{cosz2}
Te1	0.0014(3)	0.0029(2)	0.016(3)	−0.0013(3)	−0.0014(1)	−0.0059(4)
Te2	−0.0002(2)	0.0022(2)	−0.0006(2)	0.0013(3)	−0.0007(1)	0.0044(3)
Br	0.0003(2)	0.0011(2)	0.0005(4)	−0.0024(2)	0.0027(4)	−0.0091(3)

[a] The position of each atom is modulated with the function of the form $\Delta\chi(v) = \sum_{i=1}^{n=1} S_{sinxi}\cdot\sin(2\pi iv) + C_{cosxi}\cdot\cos(2\pi iv)$, $v = \vec{q}\cdot\vec{r}$.

Table 6. Crenel occupation modulation function parameters of the O6 site. These parameters (Δ_0, x_4^0) give the region along the x_4 axis in which the O6 site is occupied. Δ_0 is the step width of this region, and x_4^0 is the center of this region.

Atom	Δ_0	x_4^0
O6	0.57(1)	0.246(5)

In an attempt to obtain better data and, in particular, stronger satellite reflections of **II**, an additional single-crystal X-ray measurement with longer exposure time was carried out. However, the incommensurate crystal was too sensitive and the ordering was lost by longer exposure to the beam ($\lambda = 0.71069$ Å).

Comparison of I and II: To compare the two compounds in the simplest possible way, **I** can be considered as a limiting case of the modulation as the q vector goes to zero. In this case the amplitude of the modulation of the most strongly affected, Br position corresponds to the difference in x parameters for two adjacent two Br positions. These x parameters of 0.73 and 0.79 give a difference of about $0.06\,a$, and the effective amplitude is half of that, 0.3. The amplitude of modulation in **II** is to a first approximation given by the dominant sine term of 0.044. For the normal factor of $1/\sqrt{2}$ for the effective amplitude of a sine wave, this corresponds to 0.31, a very similar value. Let us next turn our attention to position O11 in **I**. All other positions in **I** occur in pairs related by the pseudo-monoclinic symmetry, but O11 occurs without such a partner. In **II**, the number of positions is reduced because of the 3+1 dimensional symmetry that again links the atomic positions pairwise; Ba1 and Ba2 in **I** merge to Ba1 in **II**, Br1 and Br2 in **I** merge to Br1 in **II** and so on. Since O11 lacks a pairing partner in **I**, the corresponding position in **II**, O6, is partially occupied. For a modulated description of **I**, this partial occupancy would amount to exactly $^1/_2$, and in **II**, the value is similar but refines to a slightly higher value of 0.57. It indeed appears probable that the over-occupancy is coupled to the length of the $\boldsymbol{q}$ vector, which measures the distance between layers that have enhanced oxygen occupancy and is close to $1/16\,\boldsymbol{c}^*$. If the correlation were perfect, the oxygen occupancy would be 0.5625, and this target value is certainly within the scope of the experimental accuracy. If the O6 occupancy is adjusted to this value, the thermal displacement remains largely unchanged. The corresponding reduction of the O6 occupancy (to 0.4375) leads to nonphysical thermal displacement parameters. While the magnitude of the deviation of occupancy of O6 from $^1/_2$ is subject to a large uncertainty, the sign of this deviation is unambiguously positive. It is notable in this context that at ambient temperature the volume of the modulated compound is slightly smaller than that of the normal compound. The difference is slight, but it may be interpreted as the result of the interplay between an expansion caused by the increased oxygen content, and a contraction caused by replacement of repulsive Br−O interactions with attractive O-H-Br interactions.

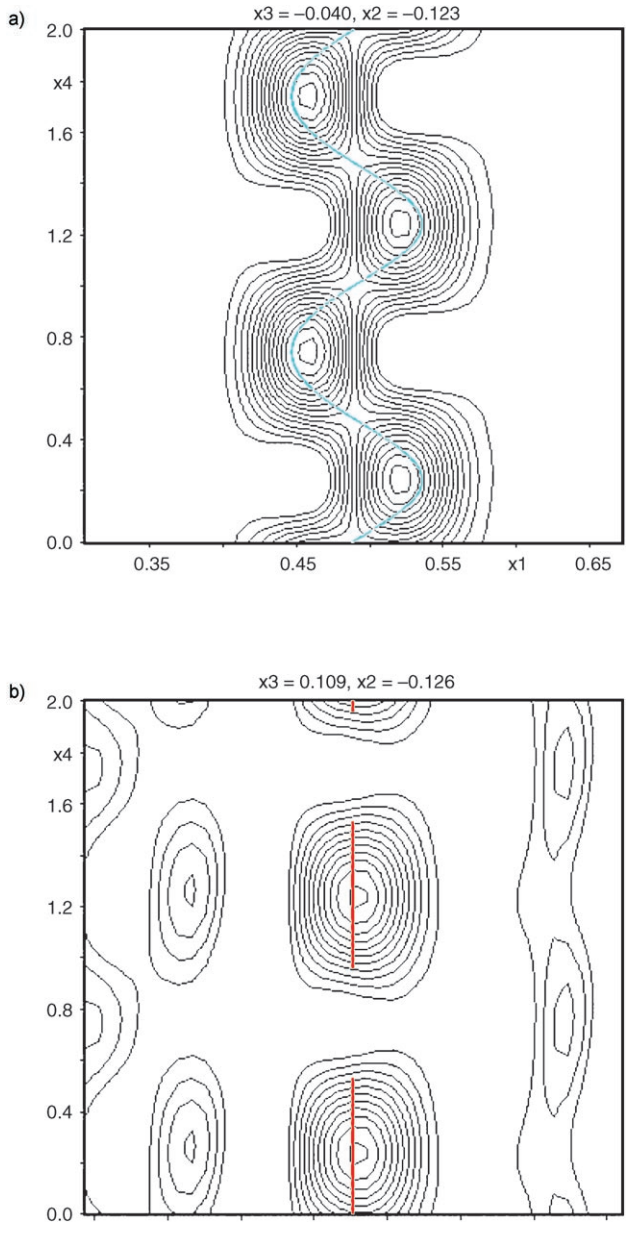

Figure 9. Calculated electron-density maps for **II**. The light blue line shows the refined modulation function of the Br atom (a) and the red line shows the refined modulation function of the O6 atom (b).

Temperature-dependent X-ray study of I: Compound **I** does not undergo any structural phase transitions in the interval from 120 to 373 K, as was proven by collecting X-ray data at these temperatures in addition to a set at ambient temperature.

Conclusion

The principal cause of the modulation of **II** appears to be the slight over-occupancy of oxygen. Its effect on the scattering is small, but the accompanying relaxation of the neighboring Br ions makes a strong contribution to the scattering power of the crystal, and the modulation becomes noticeable. The motion of the Br atom modulation can be explained by considering two situations. When a single O6 atom is situated close to the Br atom, it moves out of its way, and when the O6 atom is present on both sides of the Br atom it remains in a highly symmetric position. However, the situation is a little complicated when O6 exists on two sides. The interatomic distances between Br and O6 atoms and BVS calculation of O6 indicates substantial lowering of the valence state of O6. This can be explained by the presence of an (unaccounted for) hydrogen atom attached to O6. This also explains the higher oxygen occupancy in the modulated compound. If the modulation is indeed caused by partial replacement of O by OH, this might be promotable by synthesizing the compound in the presence of moisture. Synthesis in the presence of small amounts of water was attempted to probe this possibility, but the result was a badly ordered material in which the superstructure reflections/satellites were replaced by streaking, like that displayed by the incommensurate structure upon prolonged X-ray exposure, and no firm conclusion could be drawn.

Acknowledgement

This work has been carried out with financial support from the Swedish Research Council.

[1] a) M. Johnsson, K. W. Törnroos, F. Mila, P. Millet, *Chem. Mater.* **2000**, *12*, 2853–2857; b) R. Becker, M. Johnsson, R. Kremer, P. Lemmens, *Solid State Sci.* **2003**, *5*, 1411–1416; c) M. Johnsson, S. Lidin, K. W. Törnroos, H.-B. Bürgi, P. Millet, *Angew. Chem.* **2004**, *116*, 4392–4395; *Angew. Chem. Int. Ed.* **2004**, *43*, 4292–4295.
[2] M. G. Johnston, W. T. A. Harrison, *Acta Crystallogr. Sect. E* **2002**, *58*, i49-i51.
[3] C. R. Feger, J. W. Kolis, *Inorg. Chem.* **1998**, *37*, 4046–4051.
[4] D. Hottentot, B. O. Loopstra, *Acta Crystallogr. Sect. C* **1983**, *39*, 1600–1602.
[5] Oxford Diffraction.Xcalibur CCD system, CrysAlis Software (CCD and RED) system, Version 1.171.31.5, Oxford Diffraction Ltd, **2006**.
[6] G. M. Sheldrick, SHELXS97, Program for the solution of crystal structures, Göttingen, **1997**
[7] V. Petřícek, M. Dušek, Program for refinement of crystal structures, Institute of Physics AVCR, Praha, Czech Republic, **2000**
[8] K. Brandenburg, DIAMOND release 2.1c, Program for crystal structure graphics, Crystal Impact GbR, Bonn, **1999**
[9] J. Galy, G. Meunier, S. Andersson, A. Åström, *J. Solid State Chem.* **1975**, *13*,142–159.
[10] I. D. Brown, D. Altermatt, *Acta Crystallogr. Sect. B* **1985**, *41*, 244–247.
[11] Z. Mayerova, M. Johnsson, S. Lidin, *J. Solid State Chem.* **2005**, *178*, 3471–3475
[12] R. Attig, J. M. Williams, *Angew. Chem.* **1976**, *88*, 507–508; *Angew. Chem. Int. Ed. Engl.* **1976**, *15*, 491–492.
[13] J. Tegenfeldt, R. Tellgren, B. Pedersen, I. Olovsson, *Acta Crystallogr. Sect. B* **1979**, *35*, 1679–1682.

Received: September 27, 2007
Revised: December 17, 2007
Published online: February 21, 2008

